AGU PUBLICATIONS

JGR

Journal of Geophysical Research: Earth Surface

RESEARCH ARTICLE
10.1002/2015JF003797

Key Points:
- Feedbacks between valley wall height and channel sediment transport capacity influence vertical incision
- The inversion of a fill-cut terrace record for paleohydraulic conditions should take lateral feedbacks into consideration
- Autogenic processes due to lateral feedbacks in alluvial rivers can force accelerated incision without external forcing

Correspondence to:
L. C. Malatesta,
luca@caltech.edu

Citation:
Malatesta, L. C., J. P. Prancevic, and J.-P. Avouac (2017), Autogenic entrenchment patterns and terraces due to coupling with lateral erosion in incising alluvial channels, *J. Geophys. Res. Earth Surf.*, *122*, 335–355, doi:10.1002/2015JF003797.

Received 21 NOV 2015
Accepted 29 SEP 2016
Accepted article online 4 OCT 2016
Published online 25 JAN 2017

©2016. American Geophysical Union. All Rights Reserved.

Autogenic entrenchment patterns and terraces due to coupling with lateral erosion in incising alluvial channels

Luca C. Malatesta[1,2], Jeffrey P. Prancevic[1,3], and Jean-Philippe Avouac[1]

[1]Division of Geological and Planetary Sciences, California Institute of Technology, Pasadena, California, USA, [2]Now at Department of Earth and Space Sciences, University of California Santa Cruz, Santa Cruz, California, USA, [3]Department of Environmental Systems Science, ETH Zurich, Zurich, Switzerland

Abstract The abandonment of terraces in incising alluvial rivers can be used to infer tectonic and climatic histories. A river incising into alluvium erodes both vertically and laterally as it abandons fill-cut terraces. We argue that the input of sediment from the valley walls during entrenchment can alter the incision dynamics of a stream by promoting vertical incision over lateral erosion. Using a numerical model, we investigate how valley wall feedbacks may affect incision rates and terrace abandonment as the channel becomes progressively more entrenched in its valley. We postulate that erosion of taller valley walls delivers large pulses of sediment to the incising channel, potentially overwhelming the local sediment transport capacity. Based on field observations, we propose that these pulses of sediment can form talus piles that shield the valley wall from subsequent erosion and potentially force progressive channel narrowing. Our model shows that this positive feedback mechanism can enhance vertical incision relative to 1-D predictions that ignore lateral erosion. We find that incision is most significantly enhanced when sediment transport rates are low relative to the typical volume of material collapsed from the valley walls. The model also shows a systematic erosion of the youngest terraces when river incision slows down. The autogenic entrenchment due to lateral feedbacks with valley walls should be taken into account in the interpretation of complex-response terraces.

1. Introduction

Fluvial terraces provide records of past river geometries and can therefore be used to quantify spatial and/or temporal changes in rates of vertical incision and lateral erosion of the river. River incision and terrace abandonment can be driven by climate and tectonics, and it is typically assumed that if one of these forcings can be constrained, the terrace record may be used to reconstruct the other. Fluvial terraces are defined morphologically as a near-flat surface flanking a river, but their types vary depending on their genesis: strath terraces are cut into bedrock, fill terraces mark the culmination of an episode of alluvial deposition followed by subsequent incision, and fill-cut terraces are carved into these deposits as a river both incises and migrates laterally, leaving flights of terraces [*Bucher*, 1935; *Howard*, 1959; *Bull*, 1991; *Pazzaglia*, 2013]. All terrace types have been used for tectonic and climatic reconstructions, although both fill and fill-cut terraces (also called complex-response terraces) are less frequently employed [*Bull*, 1991; *Pazzaglia*, 2013]. For example, river terraces have been used to reconstruct past climatic conditions in Central China [*Porter and Zhisheng*, 1992], along the Rio Grande Rift in New Mexico [*Reneau*, 2000], in the American Great Plains [*Arbogast and Johnson*, 1994], in the Peruvian Andes [*Steffen et al.*, 2010; *Bekaddour et al.*, 2014], or along the Thames in England [*Maddy et al.*, 2001]. In other studies, tectonic histories have been reconstructed from the terrace record in Central Anatolia [*Schildgen et al.*, 2011], in the Apennines [*Picotti and Pazzaglia*, 2008], in the Sub-Himalaya [*Lavé and Avouac*, 2000], or across Cascadia in the northwest United States [*Pazzaglia and Brandon*, 2001]. Finally, careful examination of a single fluvial terrace record may even yield simultaneous histories of tectonics and climate, as was done in the Spanish Pyrenees [*Jones et al.*, 1999], on the South Island of New Zealand [*Bull and Knuepfer*, 1987], in the Olympic Peninsula of the northwest United States [*Wegmann and Pazzaglia*, 2002], northwestern China [*Poisson and Avouac*, 2004], or in northwest Europe [*Bridgland*, 2000].

It is often difficult to disentangle tectonic and climatic forcing in the fluvial record. This is exemplified by the conflicting interpretation of the extensive fill-cut and strath terrace record in the northern piedmont of the Chinese Tian Shan. Some authors interpret these terraces mostly as recorders of Quaternary climate change

[*Molnar et al.*, 1994; *Poisson and Avouac*, 2004; *Lu et al.*, 2010], while others attribute them to changing tectonic forcing [*Gong et al.*, 2014; *Wei et al.*, 2015]. Whether terraces are systematically linked to any discrete external forcing events, as, for example, modeled by *Hancock and Anderson* [2002], has a long history of debate: field studies [*Womack and Schumm*, 1977; *Scherler et al.*, 2016], numerical models [*Finnegan and Dietrich*, 2011; *Limaye and Lamb*, 2016], and experimental analogues [*Gardner*, 1983] have shown that internal dynamics during phases of incision can lead to autogenic strath and fill-cut terrace abandonment. Using the terrace record to infer past environmental forcing thus requires identifying the effect of autogenic processes first. Recent debate has also emerged regarding the sensitivity of incision rates to the timescale of analysis [*Finnegan et al.*, 2014; *Gallen et al.*, 2015]. *Finnegan et al.* [2014] argue that there is a systematic bias toward faster erosion rates when measuring terraces separated by shorter time intervals. They describe the bias with a negative power law dependence of incision rates on time intervals and suggest that it is the result of episodic hiatuses in erosion. In contrast, *Gallen et al.* [2015] propose that the temporal dependence results from a methodological bias that can be avoided by measuring incision rates with respect to the last abandoned terrace instead of the modern streambed given that streambed elevation is an unsteady reference frame. These two recent studies are based on long-term records of strath terraces, but do not consider complex-response terraces and the effect of autogenic processes on incision rates inferred from the terrace record.

While the fluvial terrace record is three dimensional, theories and constructs about alluvial river incision tend to be one dimensional [e.g., *Schumm*, 1973; *Leopold and Bull*, 1979; *Parker*, 2015]. Consequently, the effect of changes in channel width and lateral river migration on the terrace record is often ignored. Here we investigate whether the record of vertical incision rates in complex-response terraces can be affected by lateral feedbacks inherent to transport-limited streams. We focus on the influence of these feedbacks on the evolution of a single continuous phase of river incision in an alluvial substrate over thousands to tens of thousands of years. We assume a fixed base level and that incision is forced by a decrease in upstream sediment supply. As the channel incises vertically, we also allow it to migrate laterally and entrain sediment from valley walls. We specifically test how the contribution of sediment from valley walls affects the creation, preservation, and eventual destruction of terraces. We use a numerical model to illustrate the incision scenario and examine the internal processes leading to changes in the vertical incision rate that could be misinterpreted as externally forced. We investigate a wide range of river parameters to constrain the conditions where we expect lateral dynamics to have the greatest impact on vertical incision of the river.

2. Scenario of Alluvial Incision

2.1. Dynamics and Processes Controlling Incision

Removal of material from the bed or banks of a transport-limited river is determined by the local excess transport capacity. This is in contrast to a detachment-limited river, where sediment transport capacity is not met by the material supplied and the bed and banks are eroded at a pace limited by the bedrock erodibility. This difference makes transport-limited channels particularly sensitive to sediment inputs and the geometry of entrenchment: (1) high banks limit lateral migration and promote vertical incision [*Nicholas and Quine*, 2007] and (2) sediments delivered to the channel by bank erosion affect the transport budget of the stream [*Schumm and Hadley*, 1957; *Patton and Schumm*, 1975; *Schumm et al.*, 1984; *Meyer et al.*, 1995; *Gran et al.*, 2013]. In entrenched systems, these effects should be more pronounced. When a channel reaches the edge of its floodplain by migrating laterally, it abuts the valley wall, which is likely much taller than the river bank. When sediments derived from these valley walls are not immediately transported away, they form a talus pile, shielding the wall from subsequent erosion until their removal and potentially constraining channel width (Figure 1).

In any alluvial channel with excess transport capacity, the channel will incise its bed. However, alluvial channels are rarely static in their planform geometry, and vertical incision during a flood event may be distributed over a broader region than a single channel width as the channel moves laterally during the event. The net vertical incision of the channel is reduced when the majority of the erosion capacity is consumed by lateral migration (Figure 2a). Conversely, a channel with limited lateral migration will have a greater net vertical incision (Figure 2b). When the channel is entrenched, the lateral migration is set by the competition between the erosion of the valley wall and the pushback caused by its collapse (Figure 2c). The unlithified walls can collapse due to undercutting by the river [*Thorne and Tovey*, 1981; *Nasermoaddeli and Pasche*, 2008; *Schumm et al.*, 1984, section 6.3] and also by internal failure [*Hampton*, 2002]. The product of collapse events can overwhelm local sediment transport capacity and force aggradation of the entire channel following the

Figure 1. Talus piles shield the base of the alluvial valley walls in a tributary of the Anji Hai River, piedmont of the northeastern Tian Shan, Xinjiang Region, China (43°58′42″N/85°06′37″E).

scenario put forward by *Schumm et al.* [1984, section 6.3] and revisited in *Schumm and Rea* [1995]. However, for the bank or valley wall sediments to overwhelm the entire cross section, the channel must be narrow. Most of the time, we expect that lateral inputs of sediment from the bank or valley wall will be mobilized by the shear stress acting on that peripheral portion of the channel, while flowing water in the rest of the channel will continue incising the bed.

When valley walls are high, large talus piles encroach on the floodplain and can affect the river hydraulic geometry. After the collapse of a tall wall, it yields a volume of sediment that exceeds the local transport capacity of the portion of the river abutting the valley wall. The sediment that is not transported away forms a talus pile that encroaches on the floodplain (Figures 1 and 2c). Runoff from the terrace tread and scarp diffusion will also contribute sediment to the talus deposits. The talus has two main effects, it shields the valley wall from

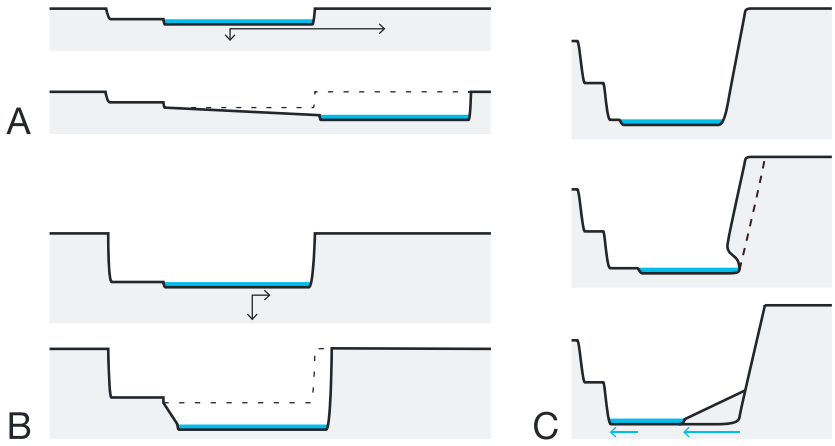

Figure 2. Processes in entrenching transport-limited rivers can promote vertical incision. In Figure 2b, valley walls are taller than in Figure 2a and limit lateral migration resulting in greater net vertical incision. (c) Bank undercut followed by a collapse that overwhelms the instantaneous sediment transport capacity results in a talus deposit pushing the river back and reducing its width. The narrower channel is deeper and its sediment transport capacity per unit width becomes larger.

fluvial erosion and it is a source of recruitable sediment. Schumm's flume work on incising channels focused on the second aspect whereby the collapsed sand and clay mixture is much more easily recruitable than the compacted sand and clay of bed and banks. It quickly saturates the river transport capacity and prevents further vertical incision [*Schumm et al.*, 1987, chapter 6]. It should also be noted that this requires talus material to be distributed over the whole channel width before entirely inhibiting the entrainment of bed material. Alternatively, when the difference in erodibility between bed and talus is small, and/or the material is not distributed across the entire channel width, the erosion of the river bed continues. In this case, the main effect of the talus is to shield the valley wall until its complete removal, thus temporarily limiting lateral migration while permitting vertical incision. In addition, when the floodplain is only marginally larger than the channel, the deflection caused by a talus deposit can constrain and reduce the channel width (Figure 2c). A narrower channel increases water depth, shear stress at the channel bed, and hence sediment transport capacity for the same slope and discharge [*Meyer-Peter and Müller*, 1948]. The sediment transport capacity can be increased this way until an optimal width occurs, below which the active bed surface for transporting sediment becomes too narrow and the total transport capacity is reduced or even reversed. Meanwhile, stresses acting on the banks are large in narrow and deep channels compared to wide and shallow geometries and erosion of the banks may proceed. As a result, this configuration is likely to be unstable and the channel will revert to a wider geometry with greater transport capacity. In the case of an incising alluvial river, ongoing vertical incision with respect to a fixed base level is necessarily accompanied by a decrease in slope. In a 1-D conceptualization, this reduction in slope would reduce the sediment transport capacity of the channel and slow the incision rate. Narrowing the river channel by lateral inputs of talus material can offset this decrease in transport capacity, and a high incision rate may be maintained or even increased as a result. The channel is trapped in a positive feedback loop in which increasing vertical incision leads to ever higher banks constraining the channel even more, reducing its width, which forces a greater vertical incision and so forth. The loop is broken when the channel reaches the equilibrium slope to transport the upstream sediment flux and cannot incise deeper. For simplicity, we neglect the negative feedback on hydraulics caused by wall effects (i.e., reduced bed shear stress due to momentum losses along the banks in channels with small width-to-depth ratios [e.g., *Parker*, 1978; *Houjou et al.*, 1990]. Accounting for this factor might alter the optimal width for maximum transport capacity but would not change the functional relationship between transport capacity and channel width in our model.

In this wall feedback process, there are two thresholds marking a significant enhancement in vertical incision of the stream. One threshold is the critical height of the valley wall, above which the material collapsing by undercut overwhelms the local sediment transport capacity of the river and forms talus piles. Above that height, lateral erosion is self-limiting and vertical incision should be enhanced. The other threshold is reached when the alluvial floodplain is so narrowed that any talus piles will reduce the width of the active channel.

2.2. Conceptual Incision Model

We illustrate the river-wall interactions with a conceptual model that forms the basis for our subsequent numerical analysis. Following a period in which an alluvial river is in equilibrium with its sediment supply (Figure 3a), vertical incision is initialized when an external forcing either reduces the river's sediment load or increases its water discharge [*Schumm*, 1973; *Leopold and Bull*, 1979]. As the channel entrains material from its bed, it also easily erodes the shallow banks and freely migrates laterally. Vertical incision and lateral erosion continue and the random lateral migration of the stream forms fill-cut terraces [*Bull*, 1991; *Limaye and Lamb*, 2016] (Figure 3b). These fill-cut terraces result from the combination of external forcing (vertical incision) and autogenic dynamics (lateral migration). Progressively, the height of the valley walls increases, the lateral erosion rate of the river against the walls is reduced by the increasing amount of sediment they yield, and the vertical erosion is distributed across a smaller area, increasing net vertical incision [*Nicholas and Quine*, 2007]. As incision continues, the episodic collapse of the ever higher walls through undercut and runoff erosion produces so much sediment that it exceeds the local sediment transport capacity at the channel margins and talus piles start accumulating at the toes of the cliffs (Figure 3c). The rivers of the north piedmont of the East Tian Shan, flowing on an unlithified fanglomerate [*Avouac et al.*, 1993], illustrate this behavior well (Figure 1). Preceding the onset of incision 10–12 kyrs ago, the rivers migrated over an expansive and steep floodplain over 2 km wide. This floodplain has since been reduced to a modern width of 200–300 m, matching the bankfull width of the channel after up to 300 m of channel entrenchment and a reduction of its slope by a factor of almost 2 [*Poisson and Avouac*, 2004]. The existing talus deposits reduce the width of the floodplain, forcing the channel to narrow with the shallowing slope [*James*, 1991; *Surian and Rinaldi*, 2003].

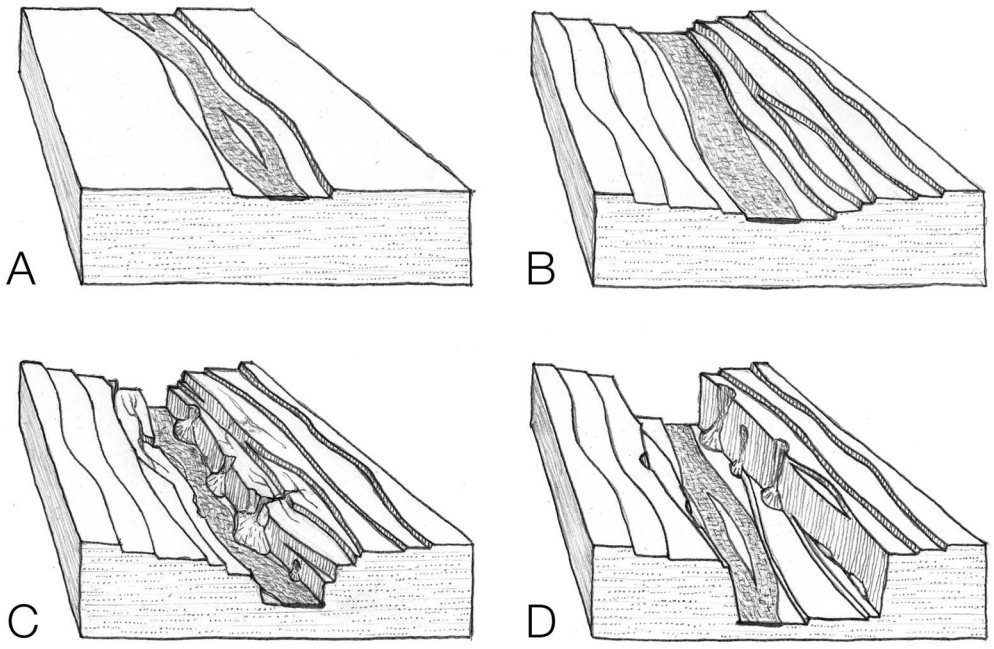

Figure 3. Scenario for the abandonment of fill-cut terraces by the entrenchment of a transport-limited river with fixed base level in an easily erodible sedimentary substrate triggered by a change in water or sediment flux from upstream: (a) at the onset of incision, short alluvial banks with relatively low resistance allow the river to easily migrate laterally; (b) migration and incision of the river result in the abandonment of autogenic fill-cut terraces; (c) taller banks slow down lateral erosion and talus deposits force narrowing of the channel. As a result, vertical incision accelerates and the stream carves a canyon; (d) after reaching a longitudinal profile close to being in equilibrium with the new upstream fluxes of water and sediment, vertical incision slows down and the river starts to migrate laterally again and to erode the youngest terraces.

Instead of a continuous slowdown of vertical incision expected from a decrease in channel slope as the river profile nears its equilibrium in a 1-D setup, we expect here a sustained vertical incision rate and even in some cases an apparent acceleration of vertical incision rates. The faster rates are unrelated to any external forcing but, rather, caused by lateral inputs of sediment from valley walls that narrow the channel and increase the shear stress over the bed. Such an acceleration could be misinterpreted as resulting from some environmental change.

Finally, when the river is near its longitudinal equilibrium and can no longer incise vertically, it will still occasionally erode the valley walls and widen its floodplain (Figure 3d). As a result, the youngest fill-cut terraces are destroyed first while the oldest terraces have a higher probability of preservation. A similar preservation bias toward older strath terraces has been demonstrated in the numerical modeling of *Limaye and Lamb* [2016]. Our model is aimed at constraining the timing and magnitude of these processes governing terrace creation and preservation.

This study fundamentally differs from knickpoint experiments in flumes where entrenchment in alluvial substrate follows from a base level drop at the downstream boundary condition of the setup (e.g., the early work of *Brush and Wolman* [1960], *Begin et al.* [1981], and *Schumm et al.* [1984]). In contrast, we use a fixed base level and the disturbance is hydraulic as the sediment transport capacity suddenly increases at the upstream boundary of the model. The relevant landform for this case is a river flowing across a piedmont over a large alluvial fan or a bajada that incises its bed after a change in climate; not an alluvial river forced by its base level. One of the key differences resides in the evolution of the sediment flux during the experiment: in a knickpoint setup, the stream is subject to an increase in sediment flux after passage of the knickpoint. But in the case of a stream that incises from a steep to a shallower gradient, the sediment flux gradually decreases as the river nears equilibrium. The works of *Schumm et al.* [1987, chapter 6], *Meyer et al.* [1995], or *Gran et al.* [2013] describe entrenched channels after the passage of a knickpoint and their reaction to lateral sediment input due to channel migration and erosion of confining alluvial walls. The results of those studies are relevant for the postincision evolution of the channels we model.

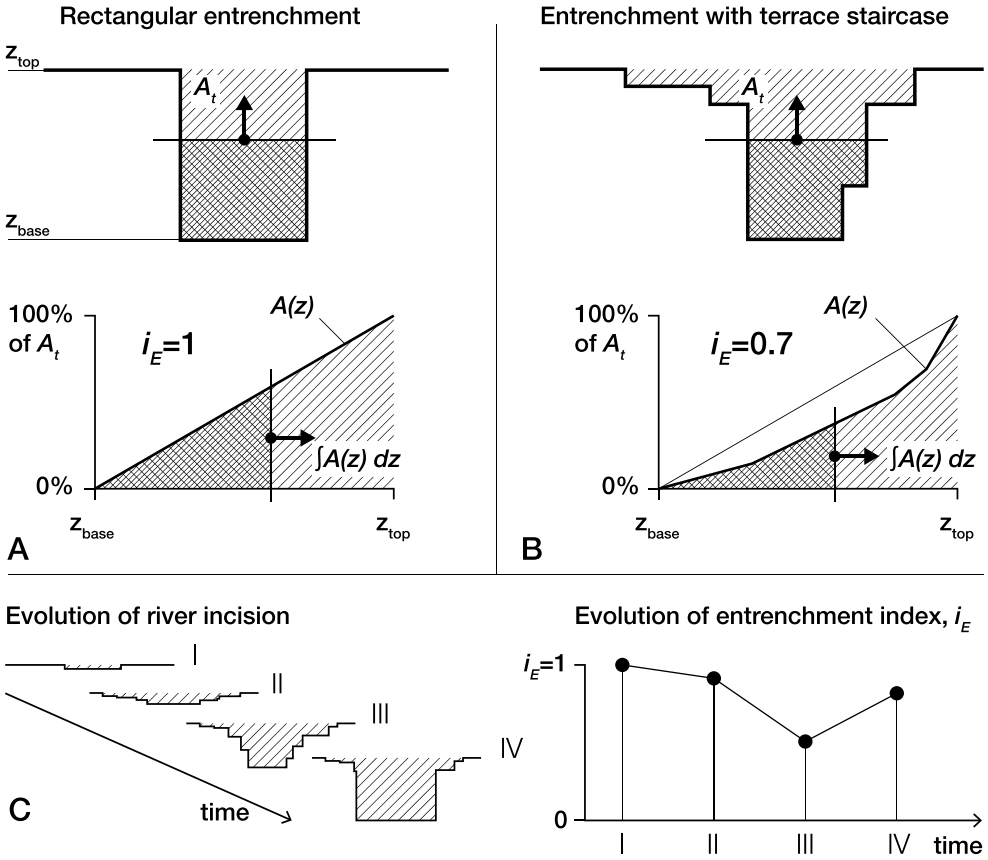

Figure 4. Illustration of the entrenchment index i_E, for (a) a rectangular canyon (top) and for (b) a stepped canyon (top). The parameter i_E is calculated with equation (1) from the normalized integral of the cumulative function recording canyon area from base to top as represented by the arrow marking the cumulative measure, $A(z)$ (cross-hatched), of the entire area, A_t (hatched, Figures 4a, bottom and 4b, bottom). (c) Scenario of valley entrenchment similar to Figure 3 and evolution of the respective i_E values.

2.3. Entrenchment Index

A rich history is recorded in the cross-sectional geometry of an incised alluvial canyon and its terraces. However, no standard metrics exist for quantifying the different geometries of a valley cross section during its incisional history (Figure 3). To cast this two-dimensional geometry into a single scalar parameter, we define an entrenchment index, i_E. The i_E is inspired by the idea of a hypsometric curve with valley width replacing elevation. The eroded area between the channel bed and the top of the highest terrace is cumulatively measured from bottom to top, $A(z)$ with $z = [z_{base} \ \dots \ z_{top}]$. The integral of $A(z)$ is then normalized by the total area of the cross section, A_t, and by the maximum elevation difference $z_{top} - z_{base}$ (Figures 4a and 4b). The normalized integral of the cumulative function is then multiplied by 2 so that its maximum value ($i_E = 1$) represents a perfect rectangular geometry (Figure 4a) and smaller values represent increasingly more funnel-shaped geometries (Figure 4b):

$$i_E = \frac{2}{A_t\,(z_{top} - z_{base})} \int_{z=z_{base}}^{z_{top}} A(z)\mathrm{d}z. \tag{1}$$

The entrenchment index allows us to quantify the geometric evolution of the valley. For example, in the scenario envisioned in Figure 3, entrenchment starts with a value $i_E = 1$ (Figure 4c, I). The index i_E decreases with the development of stepped terraces (Figure 4c, II). When the river starts to carve an entrenched canyon, the wall feedbacks engage, and i_E drops (Figure 4c, III). Eventually, as the equilibrium gradient is reached, ongoing lateral erosion progressively erases the youngest terraces from the record, leading to an increase in i_E (Figure 4c, IV).

3. Model

3.1. Setup

In the next three sections we test the entrenchment scenario (Figure 3) and the influence of the feedback mechanisms described above. We employ a simple numerical model that formalizes the essential physical mechanisms at work in a set of geometric rules. The purpose of the model is not to precisely simulate each of the complex processes occurring during fan incision: fluvial sediment transport, bank erosion, cliff collapse, and channel width evolution. Instead, the model is designed to use reasonable approximations of each of these processes in order to test how they interact over 10^3 year timescales. Every time step is an erosive bankfull event, corresponding to a characteristic flood. The code is designed to model the continuous incision of a channel in a gravel-sized sedimentary substrate. The width of the channel can only narrow in reaction to lateral constraints during entrenchment. We do not seek to model the long-term evolution of the channel which would include widening after it reaches its near-equilibrium shallower slope and erodes the valley walls. The postincisional evolution of the scenario, after the end of the model run, should however be similar to flume experiments [*Schumm et al.*, 1987] and field observations [*Meyer et al.*, 1995; *Gran et al.*, 2013] that describe deposition of alluvium on the floodplain and widening of the stream under the influx of sediment from the eroding valley walls. The model is nondimensional but we parameterize it so that dimensionalization to field values results in vertical incision rates on the order of mm/yr to cm/yr.

The model setup is a series of river cross sections. Sections are linked through their thalweg elevations that define the local stream gradient. Slope is measured with the vertical difference from one cross section to the next and the distance between channel centers in the horizontal plane. Steep alluvial rivers are often braided, but during bankfull episodes, only one or a few strands will channelize the bulk of the water in a braided floodplain; the smaller, shallower, channels do not play a significant role in shaping the floodplain geometry [*Wolman and Miller*, 1960]. We consider one single channel and not multiple strands for the sake of simplicity. During a bankfull event, a stream can incise its bed and move across its floodplain. In reality, the lateral motion depends on various fluvial processes such as braid avulsion, channel curvature, and bed morphology and is not straightforward to predict [*Knighton*, 1998, pp. 230–238]. We use an independent random-walk model in each cross section to attribute a lateral distance to be traveled by the channel during each bankfull event and to reflect the stochasticity of lateral migration. The lateral migration distance x_{lat} is chosen by a random selection from a normal distribution centered around a factor of channel width and is independently generated for each cross section. The direction of migration has equal chances to be left or right, regardless of proximity to valley walls or migration history.

The topographic nodes of each cross section are divided into four categories based on position: (1) river channel, (2) floodplain, that is, all nodes lower than a prescribed threshold height, above the thalweg, h_{FP}, (3) talus deposited after bank collapse, and (4) terraces, that is, abandoned floodplain at heights $\geq h_{FP}$. We assume that the bedload material has equal porosity in each of these settings. We ignore fine sediment (sand and finer) in our volumetric mass balance by assuming that it travels as suspended load during transport events and only occupies the interstices of coarser grains when deposited. Consequently, it is assumed to not affect bedload transport capacity or the volumetric concentration of coarser grains in any deposits. The substrate is equally erodible in all four of the cross-section elements discussed above, and the product of erosion is directly added to the sediment flux. In the floodplain nodes, pure lateral displacement has no cost for the sediment budget: in the absence of vertical incision, the product of horizontal erosion is not added to the sediment flux, but is moved to the lateral fill of the trailing bank.

The erosion that occurs during the bankfull event is set by hydraulic geometry and incoming fluxes of sediment and water. In a transport-limited river, the rate of bed erosion, E, or deposition is defined by the downstream divergence of total bedload sediment flux Qs:

$$E = \frac{\partial Q_s}{\partial x}, \tag{2}$$

where x is the downstream distance between cross sections and $Q_s = Wq_s$, that is, the channel width times the bedload flux per unit width q_s [*von Exner*, 1925; *Paola and Voller*, 2005]. The parameter q_s is determined by the nondimensional shear stress (Shields stress) acting on the bed: $\tau^* = \frac{\tau_b}{(\rho_s - \rho_w)gD}$, where τ_b is basal shear stress, ρ_s is sediment density, ρ_w is water density, D is the characteristic grain size, and g is gravitational acceleration [*Shields*, 1936]. In steady, uniform flow, the basal shear stress is $\tau_b = \rho_w ghS$, where h is water depth and S is slope. Furthermore, continuity requires that $h = Q_w u^{-1} W^{-1}$, where Q_w is water discharge, and u is flow

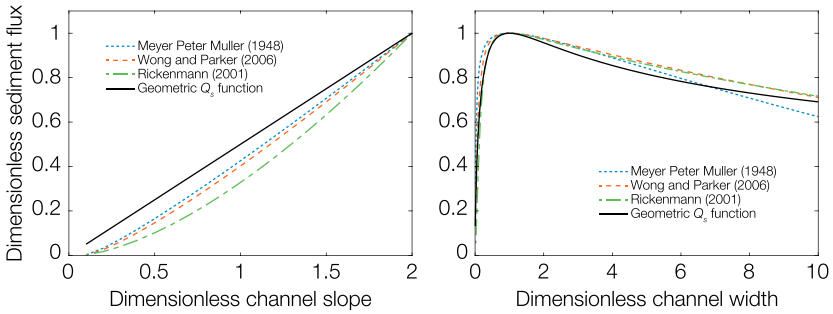

Figure 5. Comparison of the geometric sediment transport law (equation (3)) as a function of changes in slope and width with the empirical equations of *Meyer-Peter and Müller* [1948], *Rickenmann* [2001], and *Wong and Parker* [2006]. Sediment flux is normalized by the maximum transport capacity and width is normalized by the optimal width for sediment transport. The three empirical equations are calculated for a large river with (left) a fixed width of 150 m when slope varies, and (right) a fixed slope of 1% when width varies, grain size of 1 cm, and water discharge of 1000 m^3/s using the flow resistance equation of *Bathurst* [1985].

velocity. Flow velocity is typically calculated using a flow resistance equation that depends on slope, grain size, hydraulic radius ($R = \frac{hW}{2h+W}$), and/or flow depth. The q_s is then a function of the geometric terms (channel slope and width), material terms (grain size and density), and of the hydraulic terms (water discharge, velocity, and flow depth).

Using mechanistic equations for sediment transport would require parameters that are absent in a simple geometric model where only channel slope and width are resolved. So instead, we build geometric equations that mimic the dependency of Q_s on S and W, assuming all other parameters constant. The range of sediment transport we model is that of a condition largely exceeding the threshold of transport, and we assume a linear slope dependency, ignoring the threshold behavior. The resulting sediment flux equation takes the form

$$Q_s = k_A k_w \frac{S}{S_i} Q_{s_i}, \tag{3}$$

with

$$k_w = k_{\text{norm}} \frac{W^v}{\left(W_o \frac{u-v}{v} + W\right)^u}, \tag{4}$$

which mimics the empirical equations of *Meyer-Peter and Müller* [1948], *Rickenmann* [2001], and *Wong and Parker* [2006] as discussed below. Equation (3) predicts bed load transport relative to initial values of channel slope, S_i, and transport capacity, Q_{s_i}. The sediment flux is modulated with the erosivity coefficient, k_A, that accounts for the parameters that are not explicitly treated in the geometric model such as strength and duration of the flood as well as grain size. The width function $k_w(W)$ specifies how the sediment transport rate changes as a function of width. The optimal width, W_o, offers the maximum total sediment transport capacity, and k_w is a function that takes the form of a gamma distribution (equation (4)). The k_{norm} is a normalization coefficient that sets $k_w = 1$ when $W = W_o$. The coefficients $u = 0.9$ and $v = 0.6$ in equation (4) are chosen so that the width dependency of equation (3) fits the trends predicted by the empirical equations of *Meyer-Peter and Müller* [1948], *Rickenmann* [2001], and *Wong and Parker* [2006] (Figure 5). The sediment transport law we employ is calibrated against values of channel slope ranging from 0.1% to 2%, channel width from 1 to 1000 m, grain size of 1 cm, and water discharge of 1000 m^3/s.

The model is built for phases of incision. Until the gradient is near equilibrium, we do not expect sediment deposition. In the case where $\partial Q_s/\partial x$ becomes negative, which is very rare in these rapidly incising conditions, we bypass sediment to the downstream boundary. This way we avoid modeling the evolution of width during an aggradation episode and keep the simple framework of occasional narrowing toward optimum width.

For our incision scenario with lateral valley wall inputs (Figure 3), the expected changes in the two geometric parameters are shallowing of the stream gradient and potential narrowing of the width relative to their initial values, S_i and W_i. All cross sections start with the same initial values of width (W_i) and slope (S_i), and the first cross section of the model is fed with a sediment input from upstream, $Q_{s_{\text{in}}}$. At equilibrium, the model will have a transport capacity matching the incoming $Q_{s_{\text{in}}}$ in all cross sections. To promote erosion, we use a

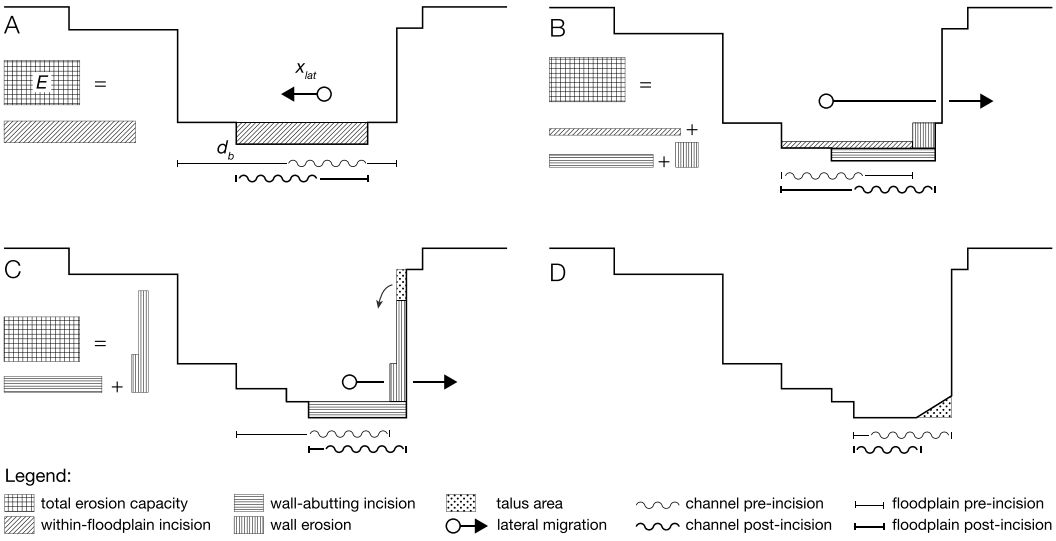

Figure 6. Step by step illustration of the model evolution. (a) At the first step, lateral migration x_{lat} is a small jog to the left and the channel is confined within the floodplain. The area to be eroded E is represented by the cross-hatched rectangle to the left and is distributed under the channel migration path. (b) At the second time step, the lateral migration is a larger step to the right. The channel incises the floodplain until meeting the valley wall. Then erosion is partitioned between terrace erosion and bed incision. The bank is short and the product of erosion by successive undercutting can be immediately evacuated. (c) Lateral motion continues to the right. The channel now undercuts a taller cliff and it cannot immediately remove the entire product of cliff erosion from undercutting. (d) The rest of the material (stippled pattern) is deposited as a talus pile at the base of the cliff and forces the channel to narrow.

value of $Q_{s_{in}}$ that is 4 times smaller than the initial transport capacity of each cross section, Q_{s_i}. The erosion E at every time step is expressed in the model space as a surface area of the cross section. In a given cross section, the lateral distance traveled by the stream, x_{lat}, sets the stretch across which the eroded area E is distributed. Figure 6 shows how erosion is formalized in the geometric model in three successive time steps. When the stream is confined within the floodplain, x_{lat} is smaller than the distance d_b between the valley wall bounding the floodplain and the river on its migrating side (Figure 6a). In this case, the entire erosion capacity E is distributed evenly across the lateral path to reflect vertical incision under the channel bed and erosion of the channel bank such that the depth of vertical incision is

$$I_1 = \frac{E}{x_{lat} + W}, \quad \text{for } x_{lat} < d_b. \tag{5}$$

When the prescribed lateral displacement is greater than the distance to the valley wall, $x_{lat} > d_b$, the stream moves against the edge of the floodplain and starts eroding the terrace riser, with the total erosion partitioned between floodplain-confined and terrace-abutting erosion along the ratio d_b/x_{lat} (Figure 6b). Vertical incision during migration across the floodplain remains I_1. Terrace-abutting erosion is split between vertical incision E_2 and lateral erosion E_3, such that the total erosion is

$$E = \underbrace{E\frac{d_b}{x_{lat}}}_{E_1} + \underbrace{\lambda E\left(1 - \frac{d_b}{x_{lat}}\right)}_{E_2} + \underbrace{(1-\lambda)E\left(1 - \frac{d_b}{x_{lat}}\right)}_{E_3}, \quad \text{for } x_{lat} > d_b. \tag{6}$$

The factor λ, between 0 and 1, sets the proportion of sediment transport capacity available for vertical incision of the bed when the river is simultaneously horizontally eroding a valley wall ($\lambda = 1$ prescribing only bed incision and $\lambda = 0$ prescribing only wall erosion). We choose here a value of $\lambda = 0.7$ for all runs, which means that when the channel erodes a valley wall, 70% of its transport capacity continues to incise the bed and 30% removes wall material. We do not explore different values of λ here, but future investigation is warranted as the partitioning of vertical and lateral erosion is an important parameter for valley wall feedback. The horizontal distance eroded into the wall depends on the lateral erosion budget of the stream and the mean height of the valley wall. In the model, the mean height is defined over a distance calculated iteratively until the eroded area

Table 1. List of Model Parameters and Their Field Equivalents

Symbol	Name	Natural Equivalent or Driving Process
k_A	Erosivity coefficient	Magnitude of bankfull event
$x_{ucut,max}$	Maximum undercut forcing cliff collapse	Strength of the bank material
W_i	Initial width of the channel	Width of bankfull channel at incision onset
x_{lat}	Lateral channel migration	Rate of channel migration across floodplain
h_{FP}	Floodplain relief	Height of bankfull stage above thalweg

corresponds to E_3. However, the lateral distance eroded into valley walls is always smaller than the distance that the stream would have traversed across its floodplain had it not encountered any obstacles.

Because the unlithified sediment of the valley wall has some cohesive strength, we assume that erosion of the valley wall does not occur continuously as the river undermines this sediment. Instead, sediment collapses into the river in pulses after lateral erosion has sufficiently undercut the valley wall [*Thorne and Tovey*, 1981]. That critical depth of undercut for wall collapse is parameterized as x_{ucut} in the model. For short valley walls, we assume that x_{ucut} is limited by the tensile strength of the cantilevered block of sediment and scales with the height of the valley wall [e.g., *Kogure et al.*, 2006]. Crudely, we prescribe the critical depth of undercut as a fraction of valley wall height for short walls ($x_{ucut} = 0.055H$). Once valley walls exceed some critical height that is determined by its cohesive strength, the undercut depth reaches a maximum $x_{ucut,max}$, which becomes the critical value for failure.

Lateral erosion thus occurs stepwise during the flood event in cycles of undercut and collapse. It proceeds by increments equal to x_{ucut} until the eroded area meets or exceeds E_3. The eroded area in excess of E_3 is then deposited as talus at the foot of the cliff (Figure 6c). The talus can constrain the channel in its floodplain and effectively reduce its width (Figure 6d). We assume that channel width tends unidirectionally toward the optimal width W_o for a maximum transport capacity at a given slope [*Lavé*, 1997]. There is no mechanism for channel widening or floodplain aggradation in the model and the channel cannot narrow below W_o to avoid scenarios warranting widening and/or aggradation. For the same reason, once a constraining talus pile is cleared from the floodplain, the channel does not revert back to its former width. In reality we expect transient phases of aggradation to restore full transport capacity when $W < W_o$. To keep the model simple we ignore this transient effect. Vertical incision occurs at a slower rate when eroding a cliff because part of the transport capacity is dedicated to sediments yielded by the wall. But the channel, limited by the pace of valley wall erosion, stays in the same location, resulting in a deeper wall-abutting vertical incision I_2:

$$I_2 = \lambda \frac{E}{W + x_{bank}} \left(1 - \frac{d_b}{x_{lat}}\right). \tag{7}$$

Our model can be reduced to one dimension by switching off lateral displacement ($x_{lat} = 0$) to prevent interactions with the banks and narrowing of the channel. Thus, we can compare the effects of lateral dynamics on vertical incision rates with the predictions of widely used 1-D frameworks [*Parker*, 2015].

3.2. Parameter Exploration

We explore the impact of five parameters that represent the main elements controlling river incision in the model: (1) the erosive potential of the bankfull event, represented by the erosivity coefficient k_A, (2) the maximum depth of undercut before bank collapse $x_{ucut,max}$, (3) the initial width of the river W_i, (4) the lateral mobility of the channel in the floodplain x_{lat}, and (5) the height above the river past which abandoned floodplain becomes terrace (Table 1). The range of values of these parameters is inspired by the rivers flowing on the north piedmont of the East Tian Shan. The dimensionalization of the runs with meters for length units and years for timestep units results in river segments that are 30 km long, with an initial slope of 2% and incising at rates of mm/yr to cm/yr over 2000 to 8000 years, similar to these Tian Shan rivers. We systematically investigate the effect of the parameters on vertical incision patterns.

The erosivity coefficient k_A is a proxy for the intensity and the duration of a bankfull event. If the bankfull events are very powerful and cause significant erosion during each flood, k_A is large. If they have a moderate magnitude and erosion occurs by smaller increments, k_A is smaller.

The maximum undercut depth that a bank or a wall can support before failure is a proxy for its strength. As described in the previous section, the critical undercut depth for collapse scales directly with the height of

Table 2. List of Simulations and Parameters[a]

Run	W_i (L)	x_{lat} (L)	k_A (1)	$x_{ucut,max}$ (L)	$h_{FP}(L)$
1	600	4*W*-3*W*	0.7	20	2
2	200	4*W*-3*W*	0.7	20	2
3	400	4*W*-3*W*	0.7	20	2
4	800	4*W*-3*W*	0.7	20	2
5	600	0.5*W*-0.5*W*	0.7	20	2
6	600	2*W*-2*W*	0.7	20	2
7	600	6*W*-4*W*	0.7	20	2
8	600	4*W*-3*W*	0.1	20	2
9	600	4*W*-3*W*	0.4	20	2
10	600	4*W*-3*W*	1	20	2
11	600	4*W*-3*W*	0.7	5	2
12	600	4*W*-3*W*	0.7	10	2
13	600	4*W*-3*W*	0.7	30	2
14	600	4*W*-3*W*	0.7	20	0.5
15	600	4*W*-3*W*	0.7	20	1
16	600	4*W*-3*W*	0.7	20	4
17	600	0.5*W*-0.5*W*	0.1	20	0.5
18	600	6*W*-4*W*	1	20	4
19	600	2*W*-2*W*	0.1	20	1
20	600	4*W*-3*W*	0.2	20	2
21	600	4*W*-3*W*	0.3	20	2
22	600	4*W*-3*W*	0.5	20	2
23	600	4*W*-3*W*	0.05	20	2
24	600	4*W*-3*W*	0.08	20	2
25	600	4*W*-3*W*	0.03	20	2
26	600	0.5*W*-0.5*W*	0.1	20	2
27	600	2*W*-2*W*	0.1	20	2
28	600	6*W*-4*W*	0.1	20	2
29	600	4*W*-3*W*	0.1	20	2
30	600	4*W*-3*W*	0.1	5	2
31	600	4*W*-3*W*	0.1	10	2
32	600	4*W*-3*W*	0.1	30	2
33	600	4*W*-3*W*	0.1	50	2
34	600	4*W*-3*W*	0.1	1	2
35	600	4*W*-3*W*	0.1	2	2
36	600	4*W*-3*W*	0.2	5	2
37	600	4*W*-3*W*	0.2	10	2
38	600	4*W*-3*W*	0.2	15	2
39	600	4*W*-3*W*	0.2	30	2
40	600	4*W*-3*W*	0.2	2	2

[a]Every parameter set is run 9 times. W_i: initial channel width; x_{lat}: mean and 1 standard deviation lateral movement as a function of channel width W; k_A: erosivity parameter; $x_{ucut,max}$: maximum undercut depth necessary for cliff collapse; and h_{FP}: floodplain relief. The units of length are arbitrary.

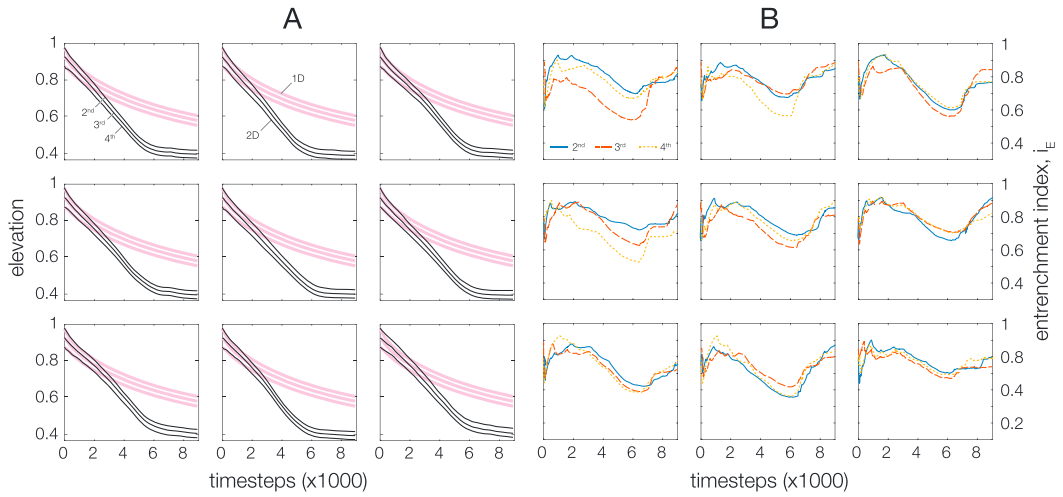

Figure 7. Nine repeated simulations of run 19 (Table 2) with identical parameters that illustrate the variability of the random walk. (a) Time evolution of the elevation of the second, third, and fourth cross sections from upstream in black. The *y* axis is normalized by the maximum height of the cross section. The pink lines show, for reference, the same runs without lateral migration, effectively 1-D simulations. (b) Evolution of the entrenchment index for the same three cross sections during the model run time.

the wall as a function of tensile strength ($x_{ucut} = 0.055H$) until a maximum undercut value, $x_{ucut,max}$, is reached for tall cliffs (set by cohesive strength), at which point the cliff collapses. A small value represents a weak lithology, e.g., loose sand, while a large value reflects stronger material, e.g., cemented conglomerate, capable of supporting a significant undercut at its base. Larger undercut depths result in larger talus piles.

The initial width of the river depends on the local history of the stream and its condition at the onset of incision, as inherited from the latest phase of aggradation or sediment bypass. This initial condition governs how much channel narrowing can happen during entrenchment.

The parameter x_{lat} sets the cross-stream distance covered by the migrating channel, if it remains within the floodplain and does not erode valley walls. If the channel erodes valley walls, then the migration distance is limited by the erosion capacity of the stream. The random walk underlying x_{lat} is designed to reflect the stochasticity of all processes during lateral migration. In addition, the mean of the distribution of x_{lat} reflects the resistance of the floodplain to lateral erosion and the duration of the bankfull event, with large migration corresponding to high erodibility and/or long events.

A surface abandoned by the channel becomes a terrace when it rises above the prescribed topographic relief of the floodplain: h_{FP}. In the model, that transition determines when the undercut of valley walls (i.e., terrace risers) engages. The relief of a floodplain is expected to scale with the flow depth of a bankfull event and the size of the sediments.

3.3. Simulation Procedure

We tested 40 sets of parameters in 360 simulations to assess the sensitivity of the model. Each of the five parameters k_A, x_{lat}, h_{FP}, $x_{ucut,max}$, and W_i is varied systematically while the others are held constant (Table 2). In addition, we ran three sets of simulations where variables covary to illustrate the end-member cases. We monitor the model evolution by recording vertical incision at every cross section and geometry of entrenchment (with i_E, Figure 4). Simulations are run 9 times with each parameter configuration to account for the variability due to the random walk controlling lateral migration (Figure 7).

4. Results

To illustrate the model setup and the breadth of dynamics it captures, we present two end-member simulations in Figure 8 (runs 19 and 18, see Table 2) and Figure 9 (run 18). The left side of Figures 8a–8d is a simulation with relatively weak hydraulic parameters: reduced erosivity k_A, low floodplain relief h_{FP}, and small characteristic lateral migration x_{lat} (run 19). The result is an extensive series of abandoned terraces in the deeply incised upper reach that turns into a wide floodplain downstream as the channel nears base level (Figure 8a).

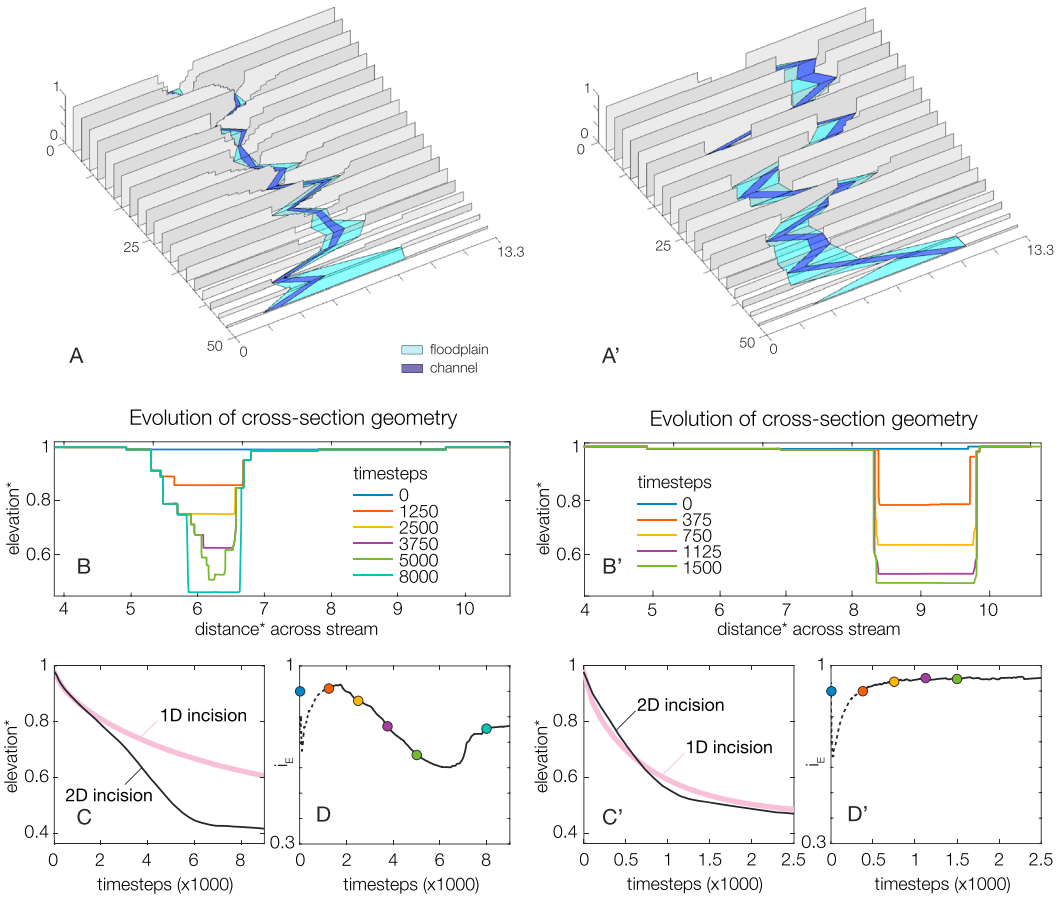

Figure 8. Two simulations capturing the end-member behavior of the model with, respectively, (a–d) low- and (a′–d′) high-intensity bankfull events represented by low or high erosivity of the bankfull flood k_A, floodplain relief h_{FP}, and channel migration x_{lat} (runs 19 and 18 in Table 2). (a and a′) Geometry of the model when the channel gradient is near equilibrium after slowdown of the incision rate (at time steps 7000 and 1500, respectively). The three axes are normalized by the total height of the model in the z dimension. (b and b′) Evolution of the second cross section from upstream through time, starting with the initial geometry at $t = 0$. (c and c′) Elevation of the channel in the second cross section through time in black; the pink line represents the same experiment without lateral migration of the channel, effectively a 1-D simulation. (d and d′) Evolution of the entrenchment index i_E through time for the second cross section. The initial drop due to shallow incision in a floodplain flanked by short walls is ignored and marked by a dotted line.

The great number of terraces (illustrated by the time evolution of the second cross section from upstream in Figure 8b) is the product of the channel's inability to efficiently erode its banks due to low k_A (low discharge) and low x_{lat} (short bankfull events). The limited transport capacity of bankfull events means that the thresholds for talus deposition and channel narrowing are reached early on. It leads to an acceleration of the vertical incision rate that departs starkly from the monotonic slowdown of vertical incision observed if the same experiment is run with $x_{lat} = 0$, effectively a 1-D simulation (Figure 8c). The longitudinal profile evolution of the same run is shown in Figure 9. The narrowing of the channel and its floodplain and the abandonment of stable terraces have a characteristic geometric signature captured by the entrenchment index i_E in the second cross section from upstream (Figure 8 d). The i_E decreases as the funnel shape of the cross sections is accentuated by enhanced vertical incision and increasingly reduced lateral erosion until the gradient reaches near equilibrium (stabilization of the channel elevation in Figure 8c). The vertical incision slows down to zero as the river approaches its equilibrium gradient. Meanwhile lateral migration of the channel continues and eventually erodes valley walls and terraces (youngest first). The i_E then increases again toward one, the value for a perfectly rectangular cross section.

The right side of Figures 8a′–8d′ illustrates the opposite end-member scenario where the hydraulic parameters are relatively strong: large erosivity k_A, significant floodplain relief h_{FP}, and long characteristic lateral migration x_{lat}. The high sediment transport capacity can easily remove material collapsed from the valley

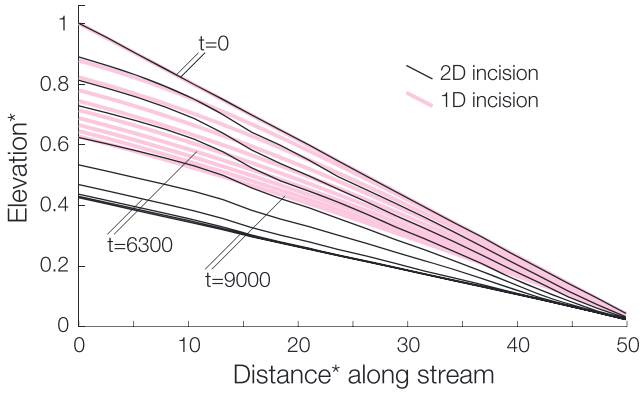

Figure 9. Longitudinal profile evolution of run 19 (Figures 8a–8d and Table 2) from $t = 0$ to $t = 9000$ with one profile every 900 time steps. The black lines show the model with lateral migration and the pink lines represent a 1-D model with lateral migration switched off. The x and y axes are normalized by the maximum height of the model.

walls. The few abandoned terraces are eroded quickly and have a short lifetime, because the river erodes the terrace risers easily, sustaining a wide floodplain and little reduction in channel width (Figures 8a′ and 8b′). While the vertical incision pattern of this simulation resembles that of the 1-D reduction (Figure 8c′), we note that vertical incision in the 2-D model initially lags the 1-D case and later overtakes it when the slight channel narrowing that does occur provides additional transport capacity to reach a shallower equilibrium slope, i.e., lower elevation. In this case the thresholds that lead to deposition of talus piles, narrowing of the channel, and enhanced vertical incision are not met early enough to make a difference.

Every parameter set has a characteristic geometry with some degree of variability unique to each run. The inherent scatter of every run is illustrated in Figure 10 where the entrenchment index i_E is quantified at the end of the main phase of vertical incision, when it reaches a minimum, before lateral erosion widens the floodplain again (see Figures 8c and 8d). Each vertical cluster in Figure 10 is composed of i_E measured at the second, third, and fourth cross sections from upstream in the nine repeat runs for a total of 27 points. We omit i_E at the first cross section to avoid boundary effects, and we limit the measurements to the upstream reach to compare cross sections with similar total vertical incision. The broad scatter of values along the y axis reflects the variability of results within one parameter set. The autogenically dominated behavior exemplified in Figures 8a–8d is primarily controlled by a reduced k_A (Figure 10a) while the parameters u_{cut} and W_i have a weak effect on i_E. A small maximum undercut depth u_{cut} limits the potential growth of talus piles and has a weak effect on i_E as well, largely within the scatter of results. A narrower initial width W_i increases the potential for fast vertical incision rates at an early stage, because it is closer to the optimal transport width (Figure 5). Additionally, as the lateral migration of the channel scales with channel width in the model, a smaller initial width will result in more frequent vertical incision episodes and the river will entrench faster (Figure 10c). Characteristic lateral migration x_{lat} and floodplain relief h_{FP} do not affect i_E. A large x_{lat} value can delay the initial entrenchment because the channel tends to sweep long lateral distances and rarely focus its incision vertically.

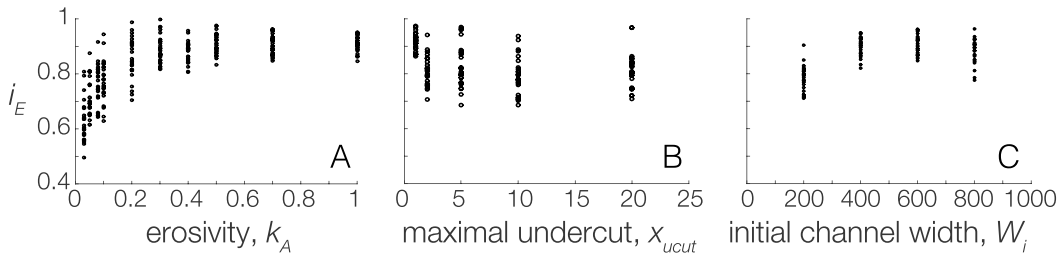

Figure 10. Sensitivity test of the model by systematic variation of one parameter and its effect on the minimum entrenchment index (captured at the end of the main incision phase, before its recovery by lateral erosion, see Figures 8c and 8d). Every cluster on the x axis is made of 27 points. Test (a) of the erosivity parameter k_A (unitless); (b) of the maximum undercut depth $x_{ucut,max}$ (L); and (c) of the initial channel width W_i (L).

5. Discussion

Our simulations show that in the simple case of a river entrenching into its former fill under constant forcing, interactions between valley wall erosion, vertical incision, and channel width evolution can lead to enhanced vertical incision, compared to the 1-D channel evolution (Figures 7–9). We present here the complementarity between our model and earlier studies before discussing the effects of the model parameters on river dynamics and vertical incision rates which inform our understanding of fill-cut terrace records.

5.1. Comparison With Earlier Studies

Two studies, in particular, by *Schumm et al.* [1987, chapter 6] and *Meyer et al.* [1995], have investigated similar fluvial geometries where a river is bound by tall valley walls of alluvium. There are fundamental differences between the forcings they considered and ours, but this earlier work sheds light on the evolution of the river after it reaches near-longitudinal equilibrium; a condition that occurs near the end of our simulations and that is only partially investigated here.

The postincisional dynamics of the present scenario should correspond to the observations of *Schumm et al.* [1987, chapter 6]. In their flume experiments, the changing boundary condition is a drop in base level that forces fast localized incision by a migrating knickpoint. As the knickpoint migrates and erodes upstream, an increase in sediment flux overwhelms the downstream transport capacity, shutting off vertical incision and promoting widening of the downstream valley. This is analogous to the valley widening that occurs in our model after the river has adjusted to its new equilibrium slope and vertical incision has stalled. In a flume experiment related by *Schumm et al.* [1987, chapter 6, p. 206], the channel reacts to a drop in base level with rapid initial incision, followed by widening of the channel and floodplain to adjust to the increased sediment flux. Unfortunately, slope changes are not precisely tracked in these experiments and it is hard to identify trade-offs between the two essential geometric adjustments of the channel that are slope and width. In our study, the changing boundary condition is an increased sediment transport capacity that leads to progressive adjustment of the channel slope from steep to shallow gradient. It is accompanied by a constantly decreasing sediment flux at the outlet: from the strong flux caused by the rapid initial erosion, to a smaller flux equal to the input from the upstream boundary condition of the model after erosion has ceased and the stream reached a new equilibrium.

Meyer et al. [1995, pp. 1227–1228] suggest that during valley widening, "the threshold of critical power for channel incision is not exceeded"; meanwhile, "a consistent supply of sediment from distal fan erosion would permit construction of a broad floodplain and inhibit degradation in the lower valley." Like the flume experiments of *Schumm et al.* [1987, chapter 6], this is the case of a channel subject to an increase in sediment flux. The river adapts its transport capacity to an increasing load and does so by widening the channel and the floodplain. This situation would again be relevant for the period that follows the entrenchment phase we model, when the channel ceases to incise with respect to its base level and widening of the valley continues. During the window of vertical incision that is the focus here, the sediment flux in the channel decreases with the sediment transport capacity as it relaxes from its oversteepened initial geometry to a shallower slope.

5.2. Effects of Parameters

The erosivity coefficient k_A appears to be the key parameter determining if the positive entrenchment feedbacks can be initiated. The k_A is a proxy for the total sediment transport capacity of a bankfull event, that is, its magnitude and/or duration. Ultimately, it is the capacity of the river to evacuate material collapsed from the valley walls that determines if and when lateral feedbacks can enhance entrenchment and lead to channel narrowing.

The characteristic lateral migration of the channel has little effect on the evolution of entrenchment. This is due to the fact that, initially, even a limited lateral motion will cause the channel to interact with the valley walls. Furthermore, it is the probability of very small migration distances that matters most. In this case, the increase in wall height is maximal and subsequent lateral erosion is that much harder. Finally, the initial width matters in that it sets the potential for stream narrowing and thereby the possible increase in sediment transport capacity relative to the initial geometry.

To synthesize the numerical exercise, we collapse the simulation results to show i_E as a function of a common nondimensional parameter k_{ND}. The key component controlling lateral feedbacks is the relationship between the volume of material produced by the eroding valley walls and the capacity of the river to remove this material. When the former exceeds the latter, significant talus deposits start shielding the banks and constraining

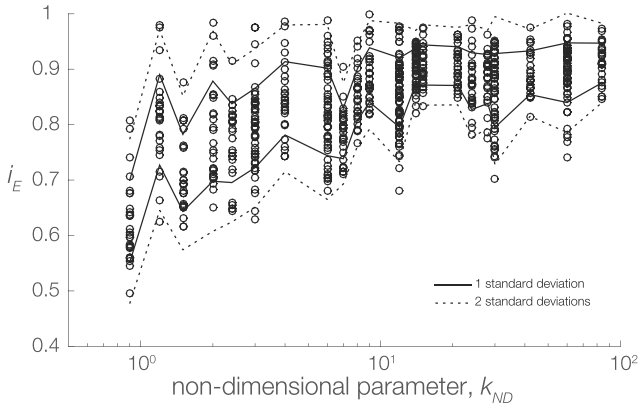

Figure 11. Minimum entrenchment index (captured at the end of the main incision phase, before its recovery by lateral erosion, see Figures 8c and 8d) as a function of the nondimensional parameter $k_{ND} = k_A W_i / x_{ucut,max}$ where k_A is the erosivity parameter, W_i is the initial channel width, and $x_{ucut,max}$ is the maximum undercut necessary for the collapse of tall cliffs for each of the runs listed in Table 2 (open circles). One and two standard deviations are drawn to indicate the trend that is partly obscured by the model stochasticity.

the channel. To reflect this first-order relation, we define $k_{ND} = k_A W_{in} / x_{ucut,max}$, so that the erosivity coefficient (dimensionless) and the width (length) across which sediment is transported are balanced by the value of the maximum undercut (length), a parameter for the volume of material shed from the valley walls. The other control on that volume is the height of the walls, but this value varies with time and cannot be treated as a model parameter. We show in Figure 11 how k_{ND} captures, albeit crudely, the sensitivity of entrenchment geometry to the parameters. The entrenchment is enhanced for smaller values of k_{ND}, reflecting the increasing importance of talus deposits.

5.3. Rate of Vertical Incision

The channel lateral dynamics affect vertical incision rates in two ways. First, the initial rate is slower than that of 1-D simulations because lateral migration consumes a portion of the sediment transport capacity that would otherwise be available for vertical incision. Second, if significant channel narrowing occurs, the increased sediment transport capacity perpetuates a rapid vertical incision rate compared to the 1-D case (Figures 8c/8c'). The equilibrium slope of the narrower channel is shallower, and the stream incises deeper into the substrate. The magnitude of the two effects vary with different parameters but they are almost always observable. Accelerated vertical incision rates also mean that deeper and older strata of the underlying substrate can be eroded and remobilized in the modern sediment flux relatively fast.

The numerical experiments illustrate the importance of the thresholds for talus deposition and channel narrowing. Autogenically accelerated vertical incision occurs when both are passed. Two quantities are in play: (1) the amount of material that can be removed from the channel during a bankfull event and (2) the volume of material that collapses from the valley walls into the channel and forms a talus pile after the budget for lateral erosion (E_3) has been consumed. The collapsed material is a function of the wall height and the critical undercut depth leading to failure and is independent from the hydraulic conditions. Under conditions of relatively low-intensity bankfull events (small k_A, x_{lat}, and h_{FP}) the channel is more sensitive to bank collapse, because small floods are only capable of removing a small portion of the collapsed material and the rest forms a talus. As a consequence, the importance of lateral feedbacks grows with reduced flood erosion capacity. In the low erosivity parameter space, channel width is thus reduced early, when the stream gradient is far from equilibrium. And so the enhanced erosion capacity due to channel narrowing impacts the system while its incision potential is still large. In this case, the decrease in transport capacity due to the shallowing slope is outweighed by the channel narrowing (Figures 5 and 9) and vertical incision can accelerate (Figure 8c). On the contrary, in the parameter space of larger erosion rates, the channel only starts narrowing when the cliffs are high and the stream gradient is already close to equilibrium, leaving little incision potential. There is then no opportunity to accelerate vertical incision, and the valley geometry remains rectangular (Figure 8c').

5.4. Terrace Record

Here we discuss how our results may best be applied to actual records of complex-response terraces under climatic and tectonic forcings, including the possible bias introduced by incision transience and selective preservation of terraces.

The terrace record is often used as a direct proxy for external forcing. Usually researchers focus on strath terraces to stay clear of the autogenic patterns that can dominate fill and fill-cut terrace records [*Schumm*, 1973; *Bull*, 1991]. It can happen, however, that both strath and fill-cut terraces share the same tread such as in the northern piedmont of the Chinese Tian Shan [*Molnar et al.*, 1994] and the Himalayan piedmont [*Lavé and Avouac*, 2000], blurring the local relevance of discriminating strath versus fill-cut terraces. Furthermore, complex-response terraces hold information that their strath counterparts often miss. They often quickly succeed each other, offering a high-resolution temporal record. In addition to their susceptibility to autogenic dynamics, fill and fill-cut terraces respond to and record external rapidly changing forcings. Indeed, *Poisson and Avouac* [2004] invert a fill-cut record to retrieve Holocene hydraulic forcing in Central Asia. Identifying and removing the incision effects of autogenic dynamics should permit the interpretation of high-resolution external forcings in a fill-cut record.

Our study shows that when autogenic feedbacks play a strong role, the entrenchment pattern recorded by the distribution of abandoned fill-cut terraces differs starkly from the actual forcing if one was to invert the vertical incision rate directly (Figure 8c). To illustrate this point, we discuss here a thought experiment with a full terrace record comprised of allogenic fill terraces and autogenic fill-cut terraces. In particular, Figure 12 shows hypothesized conditions after two cycles of incision and aggradation in an alluvial landscape in net uplift, such as a piedmontal fold-and-thrust belt. Using this conceptual model, we argue that differences in terrace generation and destruction may be deduced from entrenchment geometries and terrace ages.

Terraces are transient landforms. After a phase of incision that results in many terraces, lateral erosion continues occasionally and trims the terrace risers of the alluvial valley walls as the channel keeps migrating in its floodplain. It is noteworthy that a straight-flowing river has an equal chance (on average) of eroding either valley wall at any time while a river migrating unilaterally will preserve an entire terrace record in its wake. Younger terraces are eroded first as they border the channel and do so quickly because their height (and volume) is relatively low. This is illustrated in the short lifespan of terraces abandoned late in the incision cycle of Figure 12b (in beige). For long-term preservation, terraces first need to survive their infancy close to the river channel where the risk of erosion is highest. In the scenario where autogenic dynamics are important (illustrated by run 19 in Figures 8a–8d and 9), we observe that the older fill-cut terraces tend to be wider and this, together with their greater height, means that they take longer to be entirely eroded. The larger resistance to erosion and the lesser risk of burial make the complex-response terraces that are abandoned shortly after a transition from aggradation to incision more likely to be preserved, a bias also proposed for strath terraces [*Limaye and Lamb*, 2016]. Consequently, the available terrace record may be strongly affected by the degree of selective degradation that occurs. In Figure 12, the terrace record at time t_3 has been reworked relative to the record at time t_2, with the youngest terraces eroded. Classically, the youngest preserved terraces at t_3 in Figure 12 can be interpreted as markers of a discrete external event that forced a sudden entrenchment. But they can as well be the youngest remaining fill-cut terraces of a partially eroded record and reflect no punctual external forcing whatsoever. In contrast, in an alluvial landscape being uplifted, the vertical incision rate derived from comparison of fill terraces is likely to be free of the shorter-term cycles of incision and aggradation, often climatically driven and potentially autogenically biased. Because it records the river elevation at the same point of the cycle, it should be the closest reflection of the local tectonic uplift. When fill terraces cannot be unambiguously identified, selecting terraces separated by the period of the relevant higher-frequency forcing (e.g., 21 kyr orbital cycles) should skip the fast incision rates it drives. That record, spaced by the period of short-term forcing, is likely to reflect the long-term incision rate of the river (e.g., driven by tectonic uplift).

To assess the history of a field site with complex-response terraces, both the preserved terrace record and the potential for already eroded terraces need to be assessed. And so, while the preserved record is a straightforward observation, the likelihood of missing terraces can be indirectly estimated by establishing by how much vertical incision has slowed down and lateral erosion picked up. For example, without stratigraphic context, the terrace record at time t_3 suggests an increase in the incision rate since abandonment of the highest terrace (Figure 12e, solid line). However, the real incision history (Figure 12e, dashed line) shows that the incision rate is actually decelerating at t_3. If incision rate is decreasing, a valley with perched terraces above a deep canyon (e.g., Figures 3d and 12 at t_3) is less likely to be diagnostic of an external forcing excavating the canyon after the abandonment of the terraces. Rather, it is more likely to be a formerly stepped canyon where the youngest terraces have been eroded by the increased lateral erosion of a river as vertical incision slowed down.

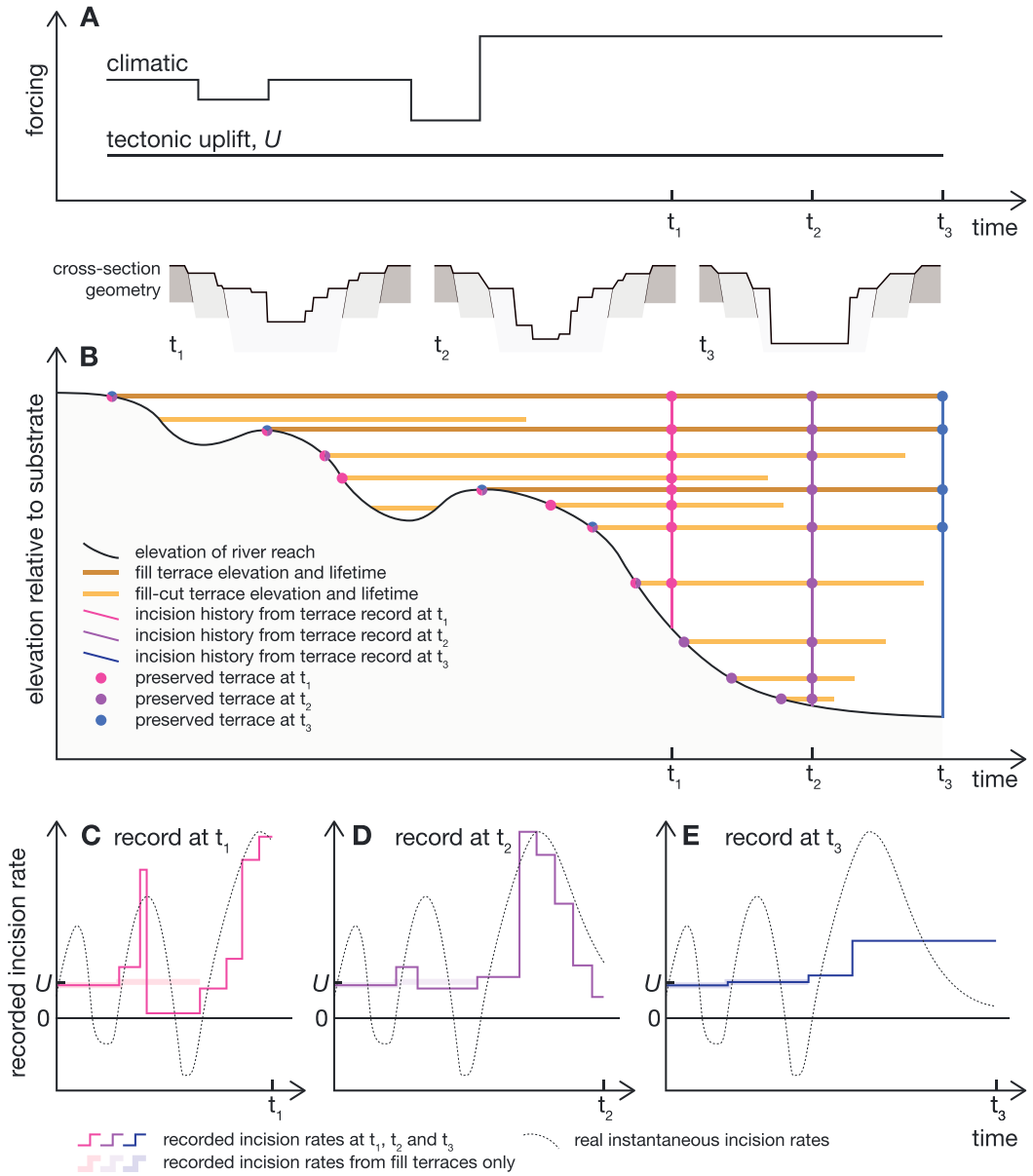

Figure 12. (a) Illustration of the model dynamics in a thought experiment of an alluvial river under the cyclic climatic forcing and constant tectonic uplift. (b) The incision and aggradation of one location along the stream in response to the forcing are shown with a black line, relative to the elevation of the material in which it incises or aggrades. The cross-sectional geometry of the valley and its stratigraphy at t_1, t_2, and t_3 are sketched above. The occasional complex-response terraces that record incision are shown as horizontal lines in Figure 12b with their elevation on the y axis and lifetime on the x axis. The terrace records at three different times (c) t_1, (d) t_2, and (e) t_3 illustrate how reconstructed incision rates (thin lines) can deviate from the real rate (dashed line) and how fill terraces (thick lines) under a similar climatic forcing can reflect uplift rate. The three time steps broadly mark the evolution of the model in Figures 3b–3d.

This simple thought experiment with complex-response terraces is reminiscent of the ongoing debate about the timescale dependency of vertical incision rates derived from the record of strath terraces [*Finnegan et al.*, 2014; *Gallen et al.*, 2015]. The potentially opposing interpretations of the two groups of authors is reflected in the evolution of the record of complex-response terraces in Figures 12c–12e. We see in our work that the preferential destruction of younger terraces may have an important influence on the incision history derived from them. *Finnegan et al.* [2014] consider the entire terrace record and observe that faster rates are systematically obtained on shorter timescales. A similar trend in the entire record is visible in Figure 12, where terraces

abandoned in quick succession (fill-cut) capture high-frequency climate forcing and yield higher incision rates than terraces farther apart. Contrary to strath terraces that are preserved over longer timescales, fill-cut terraces abandoned during the youngest episode of rapid vertical incision will be progressively truncated starting with the youngest terraces when the incision phase reaches its end. When terraces in close temporal succession are clipped off the record by erosion or burial, so are the fastest vertical incision rates. Consequently, with time, the terrace record is systematically altered and information about high-frequency forcing is lost (Figures 12c–12e). But the fill terraces, always separated by a full climatic episode, have the best chance of preservation among complex-response terraces and record the same instant of the cycle: the onset of incision at the river "highstand." *Gallen et al.* [2015] argue that deriving vertical incision rates using the youngest strath terrace as a reference instead of the river removes the bias of the transient faster rates caused by the unsteady river datum. In their model, strath terraces are abandoned at the highstand of the river incision-aggradation cycle, and since any other position of the river in the cycle is lower than the highstand, the incision rate from the youngest terrace to the river is faster than that from terrace to terrace. This is the case here as well: we obtain the long-term incision rate of the river from the fill terraces that record the river highstand position in the climate cycles and by excluding the climate forcing recorded by the successive fill-cut terraces.

6. Conclusion

Vertical incision of a transport-limited stream is prone to interactions between the channel and the valley walls. The volume of sediment collapsing from valley walls scales with their heights. Consequently, as wall heights increase, the collapsed material becomes more likely to overwhelm the local instantaneous transport capacity of the channel and form talus piles that shield banks and walls. These talus piles have the potential to constrain channel width and enhance vertical incision. This internal mechanism has a geometric signature which can be tracked with the entrenchment index i_E that quantifies the cross-sectional shape of an incised valley. Our model results suggest that this enhanced vertical incision is most pronounced in rivers with low erosivity.

Our numerical simulations also show that after a phase of vertical incision, the terrace record is progressively truncated by lateral erosion of the river starting with the youngest deposits. In a channel reaching the end of an incision phase, youngest terraces have likely been systematically eroded and the truncated record can erroneously indicate an apparent external forcing.

While this work is focused on transport-limited channels and fill-cut terraces, the dynamics resulting from the coupling of vertical and lateral erosion are probably also relevant to strath terraces that formed alongside or underneath their alluvial equivalents and potentially survived them. The interpretation of a fill-cut terrace record in terms of paleohydraulic conditions should take into consideration the effect of the valley wall feedback processes explored in this contribution.

Acknowledgments
This manuscript has greatly benefited from the remarkably thorough and precise comments of the Editor John Buffington and from insightful and engaging reviews from Frank Pazzaglia and an anonymous reviewer. We also thank Michael Lamb for his comments. This study is partly supported by a PRF New Direction grant of the American Chemical Society (grant PRF 53814-ND8), a Doc.Mobility fellowship of the Swiss National Foundation (project P1SKP2_158716) for Malatesta, NSF grant EAR-1349115 (to Michael Lamb) for Prancevic, and the donors of the American Chemical Society Petroleum Research Fund (to Michael Lamb). The source code of the model is publicly available on the web platform of the Community Surface Dynamics Modeling System (http://csdms.colorado.edu).

References

Arbogast, A. F., and W. C. Johnson (1994), Climatic implications of the Late Quaternary alluvial record of a small drainage basin in the Central Great Plains, *Quat. Res.*, *41*(3), 298–305.
Avouac, J.-P., P. Tapponnier, M. Bai, H. You, and G. Wang (1993), Active thrusting and folding along the northern Tien Shan and Late Cenozoic rotation of the Tarim relative to Dzungaria and Kazakhstan, *J. Geophys. Res.*, *98*(B4), 6755–6804.
Bathurst, J. C. (1985), Flow resistance estimation in mountain rivers, *J. Hydraul. Eng.*, *111*(4), 625–643.
Begin, Z. B., D. F. Meyer, and S. A. Schumm (1981), Development of longitudinal profiles of alluvial channels in response to base-level lowering, *Earth Surf. Processes Landforms*, *6*(1), 49–68.
Bekaddour, T., F. Schlunegger, H. Vogel, R. Delunel, K. P. Norton, N. Akçar, and P. Kubik (2014), Paleo erosion rates and climate shifts recorded by Quaternary cut-and-fill sequences in the Pisco Valley, central Peru, *Earth Planet. Sci. Lett.*, *390*, 103–115.
Bridgland, D. R. (2000), River terrace systems in north-west Europe: An archive of environmental change, uplift and early human occupation, *Quat. Sci. Rev.*, *19*(13), 1293–1303.
Brush, L. M., Jr., and M. G. Wolman (1960), Knickpoint behavior in noncohesive material: A laboratory study, *Geol. Soc. Am. Bull.*, *71*(1), 59–74.
Bucher, W. H. (1935), "Strath" as a geomorphic term, *Science*, *75*, 130–131.
Bull, W. B. (1991), *Geomorphic Responses to Climatic Change*, Oxford Univ. Press, New York.
Bull, W. L., and P. L. K. Knuepfer (1987), Adjustments by the Charwell River, New Zealand, to uplift and climatic changes, *Geomorphology*, *1*(1), 15–32.
Finnegan, N. J., and W. E. Dietrich (2011), Episodic bedrock strath terrace formation due to meander migration and cutoff, *Geology*, *39*(2), 143–146.
Finnegan, N. J., R. Schumer, and S. Finnegan (2014), A signature of transience in bedrock river incision rates over timescales of 10^4–10^7 years, *Nature*, *505*(7483), 391–394.
Gallen, S. F., F. J. Pazzaglia, K. W. Wegmann, J. L. Pederson, and T. W. Gardner (2015), The dynamic reference frame of rivers and apparent transience in incision rates, *Geology*, *43*(7), 623–626.

Gardner, T. W. (1983), Experimental study of knickpoint and longitudinal profile evolution in cohesive, homogeneous material, *Geol. Soc. Am. Bull.*, *94*(5), 664–672.
Gong, Z., S.-H. Li, and B. Li (2014), The evolution of a terrace sequence along the Manas River in the northern foreland basin of Tian Shan, China, as inferred from optical dating, *Geomorphology*, *213*, 201–212.
Gran, K. B., N. J. Finnegan, A. L. Johnson, P. Belmont, C. Wittkop, and T. Rittenour (2013), Landscape evolution, valley excavation, and terrace development following abrupt postglacial base-level fall, *Geol. Soc. Am. Bull.*, *125*(11–12), 1851–1864.
Hampton, M. A. (2002), Gravitational failure of sea cliffs in weakly lithified sediment, *Environ. Eng. Geosci.*, *8*(3), 175–191.
Hancock, G. R., and R. S. Anderson (2002), Numerical modeling of fluvial strath-terrace formation in response to oscillating climate, *Geol. Soc. Am. Bull.*, *114*(9), 1131–1142.
Houjou, K., Y. Shimizu, and C. Ishii (1990), Calculation of boundary shear stress in open channel flow, *J. Hydrosci. Hydraul. Eng.*, *8*, 21–37.
Howard, A. D. (1959), Numerical systems of terrace nomenclature—A critique, *J. Geol.*, *67*(2), 239–243.
James, L. A. (1991), Incision and morphologic evolution of an alluvial channel recovering from hydraulic mining sediment, *Geol. Soc. Am. Bull.*, *103*(6), 723–736.
Jones, S. J., L. E. Frostick, and T. R. Astin (1999), Climatic and tectonic controls on fluvial incision and aggradation in the Spanish Pyrenees, *J. Geol. Soc. London*, *156*(4), 761–769.
Kogure, T., H. Aoki, A. Maekado, T. Hirose, and Y. Matsukura (2006), Effect of the development of notches and tension cracks on instability of limestone coastal cliffs in the Ryukyus, Japan, *Geomorphology*, *80*(3), 236–244.
Knighton, D. (1998), *Fluvial Forms and Processes: A New Perspective, A Hodder Arnold Publ.*, Arnold, Arnold, London.
Lavé, J. (1997), Tectonique et érosion: l'apport de la dynamique fluviale à l'étude sismotectonique de l'Himalaya du Népal Central, PhD thesis, Univ. Paris VII, Paris.
Lavé, J., and J.-P. Avouac (2000), Active folding of fluvial terraces across the Siwaliks Hills, Himalayas of central Nepal, *J. Geophys. Res.*, *105*(B3), 5735–5770.
Leopold, L. B., and W. B. Bull (1979), Base level, aggradation, and grade, *Proc. Am. Philos. Soc.*, *123*, 168–202.
Limaye, A., and M. P. Lamb (2016), Numerical model predictions of autogenic fluvial terraces and comparison to climate change expectations, *J. Geophys. Res. Earth Surf.*, *121*, 512–544, doi:10.1002/2014JF003392.
Lu, H., D. W. Burbank, and Y. Li (2010), Alluvial sequence in the north piedmont of the Chinese Tian Shan over the past 550 kyr and its relationship to climate change, *Palaeogeogr. Palaeoclimatol. Palaeoecol.*, *285*(3–4), 343–353.
Maddy, D., D. Bridgland, and R. Westaway (2001), Uplift-driven valley incision and climate-controlled river terrace development in the Thames Valley, UK, *Quat. Int.*, *79*(1), 23–36.
Meyer, G. A., S. G. Wells, and A. J. T. Jull (1995), Fire and alluvial chronology in Yellowstone National Park: Climatic and intrinsic controls on Holocene geomorphic processes, *Geol. Soc. Am. Bull.*, *107*(10), 1211–1230.
Meyer-Peter, E., and R. Müller (1948), Formulas for bed-load transport. paper presented at 2nd Meeting of the International Association for Hydraulic Structures Research, pp. 39–64, Stockholm, Sweden.
Molnar, P., E. T. Brown, B. C. Burchfiel, D. Qidong, F. Xianyue, L. Jun, G. Raisbeck, S. Sianbang, W. Zhangming, F. Yiou, and Y. Huichuan (1994), Quaternary climate-change and the formation of river terraces across growing anticlines on the north flank of the Tien-Shan, China, *J. Geol.*, *102*(5), 583–602.
Nasermoaddeli, M. H., and E. Pasche (2008), Application of terrestrial 3D laser scanner in quantification of the riverbank erosion and deposition. paper presented at 4th International Conference on Fluvial Hydraulics, International Association for Hydro-Environment Engineering and Research, Izmir, Turkey.
Nicholas, A. P., and T. A. Quine (2007), Modeling alluvial landform change in the absence of external environmental forcing, *Geology*, *35*(6), 527–530.
Paola, C., and V. R. Voller (2005), A generalized Exner equation for sediment mass balance, *J. Geophys. Res.*, *110*, F04014, doi:10.1029/2004JF000274.
Parker, G. (1978), Self-formed straight rivers with equilibrium banks and mobile bed. Part 2. The gravel river, *J. Fluid Mech.*, *89*(01), 127–146.
Parker, G. (2015), *1-D Sediment Transport Morphodynamics With Applications to Rivers and Turbidity Currents*, Univ. of Illinois. [Available at http://hydrolab.illinois.edu/people/parkerg.]
Patton, P. C., and S. A. Schumm (1975), Gully erosion, Northwestern Colorado: A threshold phenomenon, *Geology*, *3*(2), 88–90.
Pazzaglia, F. J. (2013), 9.23 Fluvial terraces, in *Treatise of Geomorphology*, edited by E. Wohl, pp. 379–412, Elsevier, Amsterdam.
Pazzaglia, F. J., and M. T. Brandon (2001), A fluvial record of long-term steady-state uplift and erosion across the Cascadia forearc high, western Washington State, *Am. J. Sci.*, *301*(4–5), 385–431.
Picotti, V., and F. J. Pazzaglia (2008), A new active tectonic model for the construction of the Northern Apennines mountain front near Bologna (Italy), *J. Geophys. Res.*, *113*, 1–24, doi:10.1029/2007JB005307.
Poisson, B., and J.-P. Avouac (2004), Holocene hydrological changes inferred from alluvial stream entrenchment in North Tian Shan (Northwestern China), *J. Geol.*, *112*(2), 231–249.
Porter, S., and A. Zhisheng (1992), Cyclic Quaternary alluviation and terracing in a nonglaciated drainage basin on the north flank of the Qinling Shan, central China, *Quat. Res.*, *38*, 157–169.
Reneau, S. L. (2000), Stream incision and terrace development in Frijoles Canyon, Bandelier National Monument, New Mexico, and the influence of lithology and climate, *Geomorphology*, *32*(1–2), 171–193.
Rickenmann, D. (2001), Comparison of bed load transport in torrents and gravel bed streams, *Water Resour. Res.*, *37*(12), 3295–3305.
Scherler, D., M. P. Lamb, E. J. Rhodes, and J.-P. Avouac (2016), Climate-change versus landslide origin of fill terraces in a rapidly eroding bedrock landscape: San Gabriel River, California, *Geol. Soc. Am. Bull.*, *128*(7–8), 1228–1248.
Schildgen, T. F., D. Cosentino, B. Bookhagen, S. Niedermann, C. Yıldırım, H. Echtler, H. Wittmann, and M. R. Strecker (2011), Multi-phased uplift of the southern margin of the Central Anatolian plateau, Turkey: A record of tectonic and upper mantle processes, *Earth Planet. Sci. Lett.*, *317-318*, 85–95.
Schumm, S. A. (1973), Geomorphic thresholds and complex response of drainage systems, in *Fluvial Geomorphology*, edited by M. Morisawa, chap. 19, pp. 299–310, 4th Annual Geomorphology Symposium, Binghamton, New York.
Schumm, S. A., and R. F. Hadley (1957), Arroyos and the semiarid cycle of erosion [Wyoming and New Mexico], *Am. J. Sci.*, *255*(3), 161–174.
Schumm, S. A., and D. K. Rea (1995), Sediment yield from disturbed Earth systems, *Geology*, *23*(5), 391–394.
Schumm, S. A., M. D. Harvey, and C. C. Watson (1984), *Incised Channels: Morphology, Dynamics, and Control*, pp. 124–141, Water Resources, Littleton, Colo.
Schumm, S. A., M. P. Mosley, and W. Weaver (1987), *Experimental Fluvial Geomorphology*, John Wiley, New York.
Shields, A. (1936), Anwendung der Ähnlichkeitsmechanik und der Turbulenzforschung auf die Geschiebebewegung, PhD thesis, Preussische Versuchsanstalt für Wasserbau und Schiffbau, Berlin.

Steffen, D., F. Schlunegger, and F. Preusser (2010), Late Pleistocene fans and terraces in the Majes valley, southern Peru, and their relation to climatic variations, *Int. J. Earth Sci.*, *99*(8), 1975–1989.

Surian, N., and M. Rinaldi (2003), Morphological response to river engineering and management in alluvial channels in Italy, *Geomorphology*, *50*(4), 307–326.

Thorne, C. R., and N. K. Tovey (1981), Stability of composite river banks, *Earth Surf. Processes Landforms*, *6*(5), 469–484.

von Exner, F. M. (1925), Über die Wechselwirkung zwischen Wasser und Geschiebe in Flüssen. Sitzungsberichte der Akademie der Wissenschaften in Wien mathematisch-naturwissenschaftlichen Klasse. Abteilung 2a, pp. 165–203.

Wegmann, K. W., and F. J. Pazzaglia (2002), Holocene strath terraces, climate change, and active tectonics: The Clearwater River basin, Olympic Peninsula, Washington State, *Geol. Soc. Am. Bull.*, *114*(6), 731–744.

Wei, Z., J. R. Arrowsmith, and H. He (2015), Evaluating fluvial terrace riser degradation using LiDAR-derived topography: An example from the northern Tian Shan, China, *J. Asian Earth Sci.*, *105*, 430–442.

Wolman, M. G., and J. P. Miller (1960), Magnitude and frequency of forces in geomorphic processes, *J. Geol.*, *68*(1), 54–74.

Womack, W. R., and S. A. Schumm (1977), Terraces of Douglas Creek, northwestern Colorado: An example of episodic erosion, *Geology*, *5*(2), 72–76.

Wong, M., and G. Parker (2006), Reanalysis and correction of bed-load relation of Meyer-Peter and Muller using their own database, *J. Hydraul. Eng.*, *132*(11), 1159–1168.